PCCP

Accepted Manuscript

ROYAL SOCIETY OF CHEMISTRY

www.rsc.org/pccp

How the Spontaneous Insertion of Amphiphilic Imidazolium-Based Cations Change Biological Membranes: A Molecular Simulation Study

Geraldine S. Lim[a], Stephan Jaenicke[b] and Marco Klähn[c]*

[a] Institute of High Performance Computing, Agency for Science, Technology and Research, 1 Fusionopolis Way, #16-16, Connexis, Singapore 138632, Rep. of Singapore

[b] National University of Singapore, Department of Chemistry, 3 Science Drive 3, Singapore 117543, Rep. of Singapore

[c] Institute of Chemical and Engineering Sciences, Agency for Science, Technology and Research, 1 Pesek Road, Jurong Island, Singapore 627833, Rep. of Singapore

E-mail: klahnm@ices.a-star.edu.sg

Abstract

The insertions of 1-octyl-3-methylimidazolium cations ($OMIM^+$) from a diluted aqueous ionic liquid (IL) solution into a model of a bacterial cell membrane are investigated. Subsequently, the mutual interactions of cations inside the membrane and their combined effect on membrane properties are derived. The ionic solution and the membrane model are simulated with molecular dynamics in combination with empirical force fields. A high propensity of $OMIM^+$ for membrane insertions is observed, with a cation concentration at equilibrium that is inside the membrane 47 times larger than in the solvent. Once inserted, cations exhibit at a distance of 1.3 nm a weak effective attraction inside the membrane. At this free energy

minimum, negatively charged phosphates of the phospholipids are sandwiched between two $OMIM^+$ cations to form energetically favorable $OMIM^+$ - phosphate - $OMIM^+$ types of coordination. The cation – cation association free energy is 5.9 kJ/mol, whereas the activation barrier for dissociation is 10.1 kJ/mol. Subsequently, $OMIM^+$ cations are inserted into the leaflet of the membrane bilayer that represents the extracellular side. The cations are evenly distributed with mutual cation distances according to the found optimum distance of 1.3 nm. Because of the short length of the cation alkyl chains compared to lipid fatty acids, voids are generated in the hydrophobic core of the membrane. These voids disorder the fatty acids, because they enable fatty acids to curl into these empty spaces and also cause a thinning of the membrane by 0.6 nm. Additionally, the membrane density increases at its center. The presence of $OMIM^+$ in the membrane facilitates permeation of small molecules such as ammonia through the membrane, which is chosen as a model case for small polar solutes. The permeability coefficient of the membrane with respect to ammonia increases substantially by a factor of seven. This increase is caused by a reduction of the involved free energy barriers, which is effected by the cations through the thinning of the membrane and through favorable interactions of the delocalized $OMIM^+$ charge with ammonia inside the membrane. Overall, the results indicate an antimicrobial effect of amphiphilic imidazolium-based cations that are found in various common ILs. This effect is caused by an alteration of the permeability of the bacterial membrane and other property changes.

Keywords: Ionic liquid, membrane, molecular dynamics, force field, permeability, partition coefficient, umbrella sampling, imidazolium, phospholipid, free energy, ammonia

1. Introduction

Ionic liquids (ILs) are salts that exhibit low melting points and that are solely composed of ions. Charge delocalization, coupled with ion asymmetry result in melting points that are sufficiently low to keep these salts liquid below 100 °C or even below room temperature. Some advantages of ILs include chemical and thermal stability, negligible volatility and non-flammability. ILs are considered as suitable substitutes for industrial solvents, since the latter are mostly composed of volatile organic compounds (VOCs),[1] which are detrimental to the environment. ILs are highly tunable and versatile solvents,[2] since numerous cations and anions can be paired together, giving rise to a virtually infinite number of possible ILs, considering that both constituents are highly amenable to structural modifications. It has been shown that the physical and chemical properties of ILs vary widely with even simple alterations of the chemical structure of the involved ions.[3]

To date, applications involving ILs have been diverse, ranging from petrochemistry, electrochemistry, catalysis, and even biocatalysis.[1, 4, 5] In addition, it has been discovered that some ILs possess antimicrobial properties.[6-11] It has been demonstrated that cations with long alkyl chains exhibit antimicrobial activity, where the observed antimicrobial activity was directly influenced by the length of these alkyl chains. This trend has been shown in various cation classes based on imidazolium,[6, 9, 10, 12] pyridinium,[7, 13] ammonium[8, 14] and phosphonium.[14, 15] Generally, cations with longer alkyl chains exhibit greater antimicrobial efficacy, and the optimum length was found to range from 12 to 16 carbons, varying with the cation head group.[11, 16] Cations with alkyl chains that consisted of more than 16 carbons were susceptible to the so-called cutoff effect, where the antimicrobial efficacy could not be improved further with increasing chain length.[9, 17] Functionalization of cations also affects antimicrobial activity. For instance, the incorporation of polar groups into the alkyl chain lowered the antimicrobial efficacy and toxicity of the IL.[17, 18] Conversely, it has been demonstrated that the choice of the anion is less crucial, since most of the antimicrobial activity stems from the cation counterpart.[9]

The influence of aqueous IL solutions on biological membrane models has also been studied with molecular dynamics (MD) simulations. This technique has been used amply for the study of membrane models with high spatial and temporal resolution (see e.g. refs. 19-22). More

recently, also the interactions of membranes with ILs have been studied with MD simulations. Bingham and Ballone studied the interactions of 1-butyl-3-methylimidazolium cations (BMIM) paired with varying anions with a membrane bilayer of 1-palmitoyl-2-oleoyl-sn-glycero-3-phosphocholine (POPC).[23] The authors observed tail-first insertions of the cations, and structural properties of the bilayer were assessed before and after cation insertions. It appeared that BMIM – chloride and BMIM – hexafluorophosphate destabilized the bilayer, while the effect of BMIM – bis(trifluoromethylsulfonyl)imide on the membrane was inconclusive. Klähn and Zacharias investigated the insertions of 1-octyl-3-methylimidazolium cations into healthy and cancerous erythrocyte membrane models.[24] They found that the presence of cholesterol in the membranes impeded the insertion of cations. Yoo *et al.* studied the effects of IL concentration in water and cation alkyl chain length on a POPC phospholipid bilayer.[25] Spontaneous cation insertion was observed, regardless of the alkyl chain length. Our group recently published findings on the impact of insertions of 1-octyl-3-methylimidazolium and 1-tetradecyl-3-methylimidazolium cations into a membrane with a composition approximating that of the gram-negative bacterium *E. coli*.[26] It was found that both cations were absorbed spontaneously by the membrane, but also that 1-tetradecyl-3-methylimidazolium cations possessed a propensity to aggregate in solution before insertion into the membrane could be achieved. It was also found that those 1-tetradecyl-3-methylimidazolium cations that were inserted into the membrane tended to mimic the phospholipids in their vicinity.

The aim of this work is to study the effect of ion pairs from IL 1-octyl-3-methylimidazolium lactate (OMIM-Lact) in aqueous solution on a model membrane that mimics some of the key features of an external bacterial membrane. In the first part we investigate the partitioning of the cations into the membrane by deriving the change in free energy after cation insertion. Furthermore, the mutual interaction of cations after their insertion is studied and free energy simulations showed that an energetically favorable distance exists between cations inside the membrane. Based on these results, a membrane model is built with extensive cation insertions into one of the two leaflets of the bilayer. This cation-bearing membrane as well as a reference system that contains a solvated membrane without IL, are simulated with MD. Subsequently,

changes in the membrane properties induced by the inserted cations are assessed to find indications for antimicrobial activity. Considered properties involve membrane thickness, electron density profiles and lipid order parameters, among others. Lastly, changes in the membrane permeability with respect to a small polar molecule, ammonia, are studied.

2. Methods

2.1 Membrane Model

The bilayer model adopted in this work aims to represent the lipid composition of the Gram negative bacterium, *Escherichia coli* (*E. coli*), which consists of about 80 mol % phosphatidylethanolamine (PE), 15 mol % phosphatidylglycerol (PG), and 5 mol % phosphatidic acid (PA).[27, 28] The latter two lipids carry a negative charge, whereas PE is zwitterionic at physiological pH. In the membrane model, the small quantities of PA were replaced with PG to reduce the heterogeneity of the model membrane without changing the total negative charge of the bilayer surface. Increased membrane homogeneity facilitates achieving a sufficient structural sampling in free energy simulations of the membrane model. The other two types of phospholipid were incorporated into the bilayer model as 1-palmitoyl-2-oleoyl-*sn*-glycero-3-phosphoethanolamine (POPE), and 1-palmitoyl-2-oleoyl-*sn*-glycero-3-phosphoglycerol (POPG).

The CHARMM-GUI membrane builder[29-32] was used to generate the initial structure of the lipid bilayer, which consisted of 40 lipids per leaflet, i.e. 80 lipids in total. 64 POPE and 16 POPG lipids were used to constitute the membrane. The membrane model is symmetric, i.e. the same lipid composition was used in both layers. The membrane surface was chosen to be of square shape. A solvent layer consisting of 5382 water molecules was added that solvated the membrane. To ensure charge neutrality, 16 sodium ions were added to the solvent, initialized at random positions, to balance the negative charge of POPG. This initial solvated membrane structure was used for subsequent MD simulations.

2.2 Applied Force Fields

An empirical all-atomistic force field was used to calculate the potential energy with a standard functional form as described for instance in ref. 26. The force field CHARMM36[33] was used to describe the phospholipids in the membrane and the sodium ions, whose adequacy for membrane simulations has been amply verified (see e.g. ref. 34-37). To ensure consistency with the membrane force field, the considered IL in this work, 1-octyl-3-methylimidazolium lactate (OMIM-Lact), was described using the CHARMM General Force Field (CGenFF).[38] Details of the parameterization of this IL are described in our preceding work.[26] Water molecules were described with the TIP3P model.[39]

2.3 Specification of MD Simulations

All-atomistic MD simulations were performed using the simulation software GROMACS.[40, 41] The equations of motion were integrated with the leap-frog algorithm using a time step of 2 fs. Bond lengths that involved hydrogen atoms were restrained using the LINCS algorithm.[42] Full periodic boundary conditions were applied to the cuboid boxes. A Nosé-Hoover thermostat was used,[43, 44] with a target temperature of 300 K, and with a time constant of 0.5 ps. Semi-isotropic pressure coupling was applied. Coordinates in the directions parallel to the membrane surface, *x* and *y*, were scaled independently from the coordinate perpendicular to the membrane surface, *z*, using the Parrinello-Rahman barostat.[45] The target pressure was set to 1 bar and the compressibility to 4.5 x 10^{-5} bar^{-1}. Short-range interactions were evaluated explicitly up to a cutoff distance of 1.0 nm and 1.2 nm for Lennard-Jones and Coulomb interactions, respectively. Long-range effects were considered using a dispersion correction and the fast particle-mesh Ewald method for long-range electrostatics.[46-48]

The solvated membrane obtained from CHARMM-GUI was allowed to undergo relaxation to remove close contacts. Subsequently, heavy atoms of the bilayer were restrained using a harmonic potential with a force constant of 1000 $kJ \cdot mol^{-1} \cdot nm^{-2}$, while carrying out an isochoric-isothermal ensemble (NVT) simulation for a period of 0.5 ns, during which the temperature of the system was linearly raised from 0 to 300 K. Subsequently, the restraints were removed, and another 0.5 ns of NVT simulation was performed. In the next step, the membrane was

equilibrated using an isobaric-isothermal ensemble (NPT) simulation of 100 ns length, of which the last 50 ns were used for analysis purposes. The equilibrated membrane in aqueous solution without any IL represents the reference system against which other solvated membranes that contained ILs are compared.

To analyze the effect of cations on membrane properties, 10 $OMIM^+$ cations were inserted directly into one leaflet of the membrane bilayer, whereas 10 lactate anions were added to the solvent. The cations were initially placed into the membrane with an orientation similar to that observed in our preceding work.[26] All cations were inserted into one leaflet, which represents the bacterial membrane layer that is in contact with the extracellular solvent. The mutual distance between neighboring cations was chosen according to the energetically most favorable distance that minimizes the free energy, as explained in section 3.2. At this number of cations inserted into the membrane, an even distribution of cations in the entire membrane layer was ensured, while maintaining the energetically most favorable distance between neighboring cations. The resulting ion distribution is shown in Figure 1a. This membrane was simulated for 300 ns with the parameters discussed above, however, the center-of-mass of cations was restrained in z-direction with a force constant of 100 kJ mol^{-1} nm^{-2}. This restraint was necessary to avoid cation transfer into the solvent, which was observed to lead to re-insertion into the other membrane layer. Such a shift of cations to the other membrane leaflet, which faces the cytosol, is an artifact caused by the use of periodic boundary conditions. The last 100 ns period of the simulation was used to analyze the properties of the membrane.

2.4 Free Energy Calculations

Changes in free energy were calculated for the insertions of single $OMIM^+$ cations into the membrane bilayer, ΔG_{ins}, and for the association of two neighboring cations within the membrane model, ΔG_{assoc}.

2.4.1 Calculation of ΔG_{ins}

For the calculation of ΔG_{ins}, starting from the structure of the equilibrated membrane, a cation $OMIM^+$ was added to the solvent in about 1.2 nm distance from the membrane surface. After an initial equilibration period of 1 ns, with the simulation parameters discussed above, the cation was slowly pulled into the membrane. This was achieved by adding a harmonic potential as a function of the distance between the center-of-masses of the cation and the membrane bilayer, which was projected onto the z-axis, i.e. perpendicular to the membrane surface. This distance, ζ, is a reaction coordinate that describes cation insertion and was used for the following free energy calculations. During the simulation, the minimum of the harmonic potential was then slowly changed from the initial cation – membrane distance toward smaller values until cation insertion occurred. The force constant of the harmonic potential was set to 1000 $kJ \cdot mol^{-1} \cdot nm^{-2}$, whereas the minimum of that potential was reduced with a rate of 10^{-3} $nm \cdot ps^{-1}$. From the resulting trajectory, 22 structures were selected so as to cover the entire range of ζ–values. Values of ζ larger than about 3 nm correspond to cations fully solvated in water, whereas smaller values around 2 nm correspond to cations inserted into the membrane. Two neighboring structures were separated by $\Delta\zeta$ = 0.2 nm. These structures were used as starting points for 22 independent umbrella sampling simulations of 10 ns periods each, during which ζ was restrained to its respective value using a force constant of 1000 $kJ \cdot mol^{-1} \cdot nm^{-2}$. These simulations were performed with the parameters discussed in the previous section. Only the last 8 ns of the simulations were used for analysis. The pulling forces, $F(\zeta)$, were written out throughout all umbrella sampling simulations. From these simulations the potential of mean force (PMF) was derived using the Weighted Histogram Analysis Method (WHAM).[49] Errors were determined with the Bootstrap method.[50] From the PMF, the free energy profile $\Delta G(\zeta)$ can be derived according to eq. 1:

$$\Delta G(\zeta) = -\int_{-\infty}^{\zeta} \langle F(\zeta') \rangle_t \, d\zeta' \qquad (1)$$

For eq. 1, the integration is practically done from a ζ-value that represents full solvation of the solute that is sufficiently far from the membrane up to a particular value of ζ. From this free energy profile, the insertion free energy ΔG_{ins} is determined by the free energy difference between the minimum at small ζ, when the cation is fully inserted into the membrane, and the value to which the profile converges for larger values of ζ, where the cation is solvated in bulk water.

2.4.2 Calculation of ΔG_{assoc}

To obtain ΔG_{assoc} it is required to calculate the free energy differences that resulted from pulling apart two cations that were in mutual vicinity within the membrane. Additionally, the free energy for transferring one of the two cations from the membrane into the solvent is required to derive ΔG_{assoc} indirectly through a thermodynamic cycle as will be explained in section 3.2, while one of the cations remained in the membrane. The starting structure was derived from the equilibrated system in which one cation had been inserted into the bilayer with the method described in section 2.4.1. The second cation was inserted manually in the vicinity of the first cation into the membrane at an initial cation – cation distance of about 1 nm, using a similar conformation and position relative to the membrane surface as observed for the first cation. This system was equilibrated for 20 ns. Pulling simulations to generate initial structures and umbrella simulations were performed similarly as described above with the following changes:

In the case where one of the two cations was pulled from the membrane into the solvent, the reaction coordinate ζ was defined as the distance between the center-of-masses of the two cations, projected onto the z-direction, i.e. perpendicular to the membrane surface. For pulling simulations a pulling rate of 1.5 x 10^{-3} nm·ps^{-1} was used. During the pulling simulation 18 structures were written out to initialize umbrella sampling simulations. All other simulation parameters were the same as specified in section 2.4.1.

To pull the two cations apart within the membrane, a reaction coordinate χ is defined as the distance between the center-of-masses of the two cations, which was projected onto the xy-

plane, i.e. parallel to the membrane surface. A slower pulling rate of 6 x 10^{-5} nm·ps^{-1} was used so as to mitigate artificial structural perturbations in the membrane during the pulling simulations. The pulling simulation was started at a minimum distance of χ = 0.9 nm up to a maximum distance of 2.2 nm. A force constant of 3000 kJ·mol^{-1}·nm^{-2} was applied in this pulling simulation and 12 structures were used to initialize umbrella sampling simulations.

2.5 Deriving Membrane Permeability for Small Solutes

Changes in permeability of the model membrane after absorption of cations were analyzed. This was assessed by calculating the permeability coefficient with respect to ammonia, which was used as a model case for a small polar solute.

The permeability coefficient is determined by changes in free energy and diffusivity along the path of the solute through the membrane. Both properties can be derived from umbrella sampling simulations in which the reaction coordinate of the solute, i.e. the solute position with respect to the axis perpendicular to the membrane, is restrained to a series of values. This approach was developed by Marrink and Berendsen[20, 51] and an excellent description of the method is also given in ref. 52.

Free energy changes were determined the same way as described in section 2.4.1 for the insertion of cations into the membrane, with the only exception that the solute was pulled from the solvent through both leaflets of the membrane into the solvent on the other side of the membrane. The resulting free energy profile $\Delta G(\zeta)$, where ζ is the distance between the center-of-masses of the solute and the membrane, projected onto the z-direction, can be used to determine the local partition coefficient, $p(\zeta)$:

$$p(\zeta) = \exp(-\frac{\Delta G(\zeta)}{RT}) = \frac{c_{\mathrm{mem}}(\zeta)}{c_{\mathrm{wat}}} \qquad (2)$$

In eq. 2, c_{mem} and c_{wat} are the local concentration of the solute in the membrane at a reaction coordinate value ζ and the solute concentration in water, respectively.

The same pulling forces, $F(\zeta)$, that are used to derive the PMF to determine $\Delta G(\zeta)$ can also be used to derive the local diffusion coefficients, $D(\zeta)$, of the solute at different values of ζ:

$$D(\zeta) = \frac{(RT)^2}{\int_0^\infty \langle \Delta F(\zeta,t) \bullet \Delta F(\zeta,0) \rangle \, dt} \quad (3)$$

In eq. 3, the denominator contains the autocorrelation of $\Delta F = F - \langle F \rangle_t$, where $\langle F \rangle_t$ is the time averaged pulling force. The local partition coefficient and diffusion coefficient can be combined to calculate the local resistance of the membrane, $R(\zeta)$:

$$R(\zeta) = \frac{1}{p(\zeta) \cdot D(\zeta)} \quad (4)$$

The permeability coefficient is then given by eq. 5:

$$P = \left(\int_{-\infty}^{+\infty} R(\zeta') \, d\zeta' \right)^{-1} \quad (5)$$

Similar to eq. 1, the integration is practically carried out from a ζ-value that represents full solvation of the solute in the solvent on one side of the bilayer to the solvent on the other side of the bilayer. Both points are chosen sufficiently far from the membrane so that solvent/solute-membrane interactions become negligible.

The local partition coefficients, diffusion coefficients, resistance and the permeability coefficients of the membrane with respect to ammonia were calculated before and after absorption of cations. Ammonia was described with the CHARMM General Force Field (CGenFF).[38] To generate initial solute structures, the solute was pulled through both leaflets of the membrane using a force constant of 1000 kJ·mol^{-1}·nm^{-2} and a pulling rate of 1.0 x 10^{-3} nm·ps^{-1}. From these simulations, 30 - 40 starting structures were selected with a $\Delta\zeta$ difference of 0.2 nm. Two pulling simulations were done: One in direction of positive ζ and a second in negative ζ-direction. The results were averaged. In the case of the pure membrane, the results were additionally averaged over the two bilayers due to their equivalence. In contrast, the cation-bearing membrane is asymmetric, because all cations were inserted into one layer. In umbrella sampling simulations a restraint force constant of 1000 kJ·mol^{-1}·nm^{-2} was used.

The total energy and volume as a function of simulation time are shown in Figures S1-S7 of the Supporting Information for various simulations. The absence of trends throughout simulations confirms that these simulations were equilibrated.

3. Results and Discussion

3.1 Equilibrium Partitioning of OMIM$^+$ in Membrane

First, we investigated the partitioning of OMIM$^+$ cations in the membrane model by deriving the free energy of the cation as a function of the distance between cation and membrane. The free energy profile is shown in Figure 2a. By insertion of OMIM$^+$ into the membrane, the free energy was lowered by ΔG_{ins} = 9.6 ± 1.3 kJ/mol. This corresponds to a partition coefficient of $p = \frac{c_{\text{mem}}}{c_{\text{wat}}} = 47$. Insertion of the cation into the membrane is energetically favorable due to hydrophobic interactions that facilitate transfer of the non-polar cation alkyl chain from the polar solvent to the non-polar core of the membrane. Strong electrostatic interactions between the positively charged imidazolium ring and the negatively charged phosphate groups of the phospholipids stabilize the cation in the membrane additionally. This observation is in line with

previous findings that a cation transfer from water into the membrane is energetically favorable.[23, 24, 26]

The magnitude of the partition coefficient is fully consistent with our previous finding, where $OMIM^+$ inserted spontaneously into a very similar membrane model.[26] In these simulations, 14 cations out of 20 transferred from the water phase into the membrane. The initial concentration of ILs in water *before* the equilibrium is reached was $c_{0,wat}$ = 0.25 mol/l. On the other hand, at $c_{0,wat}$ = 0.25 mol/l and with a partition coefficient of p = 47 the cation concentration in the membrane would be c_{mem} = 0.245 mol/l, so that $p = c_{mem} / c_{wat} = c_{mem} / (c_{0,wat} - c_{mem}) = 0.245 / 0.005 = 47$. With average membrane thickness and surface area of d_{mem} = 4.31 nm and s_{mem} = 22.4 nm^2, respectively, the number of cations in the model membrane at equilibrium should be $n_{ins} = c_{mem} \cdot d_{mem} \cdot s_{mem} \cdot N_A = 14.2$, where N_A is the Avogadro's constant. This is indeed the number of spontaneous cation insertions that have been previously observed, which seems to indicate that these simulations were indeed close to the equilibrium and also that the calculated value of p is consistent with previous simulations.

Once inserted into the membrane, $OMIM^+$ orients itself perpendicular to the membrane surface with the alkyl chain pointing toward the membrane center. The imidazolium ring is coordinated to phosphates of neighboring lipids and remains partially solvated in water, as shown in Figure 2b. The alkyl chain is in contact with the fatty acids of the lipids.

3.2 Free Association Energy between Cations inside the Membrane

In this section, the interaction among cations after their insertion into the membrane was analyzed. To derive a free energy profile as a function of the cation – cation distance, one cation is moved with an artificial pulling force away from the other cation towards larger distances, while both cations remain inside the membrane. The details of this calculation were described in subsection 2.4.2.

The free energy profile as a function of the distance between the two inserted $OMIM^+$ cations projected onto the xy - membrane plane, χ, is shown in Figure 3. The maximum value of χ was

2.2 nm, which corresponds to about half of the box length. Larger values of χ in the free energy profile could not be achieved because of the limited simulation box size and the applied PBC. The free energy change reached a value of 10.1 ± 0.9 kJ/mol at χ = 2.2 nm. Most importantly, however, a clear minimum of ΔG at a distance of χ = 1.3 nm was obtained. This seems somewhat surprising, considering the mutual repulsion of the two positively charged cations. The membrane structure in the vicinity of the two cations at the minimum $\Delta G(\chi = 1.3)$ is shown in Figure 4. In this energetically favorable structure, the two cations are coordinated to the negatively charged phosphate groups of the neighboring phospholipids, yielding an $OMIM^+ – PO_4^- – OMIM^+$ coordination pattern.

While the free energy profile in Figure 3 revealed the existence of a minimum at χ = 1.3 nm, the maximum cation – cation distance was restricted because of the limited simulation box size. To derive the free energy change induced by an infinite separation of the two cations we considered the thermodynamic cycle (TDC) shown in Figure 5. According to this TDC, the free energy change that results from separating two neighboring cations inside the membrane, ΔG_{assoc}, can be derived from adding the free energy changes from three different processes: (1) transfer of one of the two cations from the membrane into the solvent, ΔG_1, (2) moving the transferred cation inside the bulk solvent until an infinite distance to the first cation is reached, ΔG_2, (3) and transferring this cation back from the solvent into the membrane, while remaining at infinite distance to the first cation, ΔG_3. The second term, ΔG_2, equals to zero because there are no interactions of the cation in the bulk solvent with the membrane and thus any movements of the cation in the solvent without approaching the membrane do not induce any free energy changes. The third term, ΔG_3, is identical with the free energy that has been derived in the previous section 3.1 for the transfer of $OMIM^+$ into the membrane, ΔG_{ins}, because the presence of a second cation in the membrane is irrelevant at infinite separation of the two cations. So the only term remaining to be calculated is ΔG_1.

This free energy change ΔG_1 was evaluated by extracting one of the two cations from the membrane with a pulling simulation and subsequent umbrella sampling as before. The starting structure was taken from the previous simulation at optimum χ = 1.3 nm. The resulting free

energy profile is shown in Figure 6. According to this profile, the free energy change ΔG_1 was 15.5 ± 0.7 kJ/mol. It follows that according to the TDC in Figure 5, the association free energy of the two cations in the membrane is ΔG_{assoc} = 5.9 kJ/mol. This result corroborates the finding that indeed the insertion of a cation is facilitated by the presence of another cation in the membrane in its immediate vicinity by forming a direct $OMIM^+$ – phosphate – $OMIM^+$ coordination.

To further confirm the existence of an effective association between the two cations in the membrane we repeated the calculation of ΔG_1 starting from different initial χ-values that were both smaller and larger than the optimal distance. For χ = 0.94 nm and 1.5 nm we obtained values for ΔG_1 of 13.5 ± 1.2 kJ/mol and 6.5 ± 1.2 kJ/mol, respectively, as summarized in Table 1. The corresponding association free energies of 3.9 kJ/mol and -3.1 kJ/mol, which are both smaller than ΔG_{assoc} = 5.9 kJ/mol at optimal χ, thereby confirm that an energy minimum indeed exists at $\chi = 1.3$ nm. The fact that the association free energy at 1.5 nm became negative implies that at that distance the mutual cation repulsion dominates. The extraction free energy at that distance is 9.0 kJ/mol lower than at optimum χ, which is consistent with the free energy increase of 10.1 kJ/mol at $\chi = 2.2$ nm (Figure 3).

The results presented in this section suggest that a cation at an optimal distance to a second cation in the membrane has to overcome a free energy barrier of about 10 kJ/mol to dissociate before it can diffuse further in the membrane. On the other hand, a cation diffusing inside the membrane faces a repulsive barrier when approaching a second cation before the optimal cation – phosphate – cation coordination can be achieved. This barrier is caused by mutual electrostatic repulsion of the two cations. This barrier can be estimated with the difference of the free energies at $\chi = 2.2$ nm, 10.1 kJ/mol, and at $\chi \to \infty$, 5.9 kJ/mol, relative to the energy minimum, which gives a weak 4.2 kJ/mol energy barrier. These findings are summarized in Figure 7. These results suggest that cations tend to aggregate to some extend after membrane insertion through diffusive processes to form the energetically favorable coordination pattern shown in Figure 4. It is perceivable that this increase in local cation concentration inside the

membrane can lead to added damage to the membrane. This is explored further in the following sections.

3.3 Effect of Cation Insertions on Membrane Properties

Property changes of the membrane induced by the insertion of $OMIM^+$ into one of the leaflets were addressed. For these simulations, the cations were oriented in the membrane as observed in section 3.1. Initial mutual distances between cations were chosen to be 1.3 nm according to the energetically most favorable distance. An even distribution of these cations in the membrane layer allowed for the insertion of 10 cations. An additional 10 lactate anions were added to the solvent. This system, together with a reference system that consisted of the solvated membrane without IL, was simulated for 300 ns. An example of the cation distribution after equilibrium was reached is shown in Figure 1b. The distribution of distances between cations was determined by the free energy profile shown in Figure 3, where cation – cation distances between 0.9 – 1.6 nm were readily accessible, because at these distances the free energy did not exceed the energy at the minimum at 1.3 nm by more than the thermal energy of $\frac{3}{2} k_{\mathrm{B}} T$. Properties of these two membranes are compared in the following sections.

3.3.1 Membrane Thickness, Roughness and Surface Area

The membrane thickness is defined here as the difference between the average z-coordinates of the phosphorus atoms in the two leaflets. The thicknesses of the pure and cation-bearing membranes are given in Table 2.

A slight reduction of 0.2 nm (4-5 %) in the thickness of the bilayer was noted. This is due to the fact that the alkyl chains of the inserted $OMIM^+$ are considerably shorter than the oleoyl and palmitoyl tails of the phospholipids. Thus, incorporation of the cations generated voids in the core region of the membrane, which give the long tails of the phospholipids more space to flex and curl. This in turn allows the two leaflets to approach each other, resulting in a bilayer of

reduced thickness. This effect has been previously observed and is discussed in the preceding work.[26] In the present study, however, cations were inserted only in one leaflet, thus the thinning effect was less pronounced. Density changes of the membrane with respect to the membrane normal are discussed more in the next section.

The roughness of the membrane surface, r_m, was evaluated by calculating the average deviation of the z-coordinates of each of the *n* phosphorus atom, z_i, from the average z-coordinate of all phosphorous atoms, $\bar{z}$, for each leaflet of the bilayer:

$$r_m = \frac{1}{n}\sum_i |z_i - \bar{z}| \quad (6)$$

The roughness of the membrane surface of the cation-bearing leaflet is shown in Table 2. The derived values suggest a small increase in surface roughness, indicating a slight disordering effect of the cations on the phospholipid head groups.

The total surface area and the surface area per molecule in the membrane were determined. For the latter property, each phospholipid and cation in the leaflet was considered. The results are shown in Table 2. While the total surface area increased by 9.1 % due to the insertion of the cations, the area per molecule decreased 5.4 %. This was caused by the smaller size of $OMIM^+$ compared to the phospholipids, thereby increasing the compound density in the membrane.

3.3.2 Membrane Electron Density Profiles

Electron density profiles have been commonly used in membrane studies to obtain important information on the order and distribution of membrane components. These electron density profiles can be obtained experimentally via X-ray diffraction or through MD simulations. The electron density profile shown in Figure 8 was obtained by dividing the membrane into 100 slices of equal volume along the z-axis of the system. The number of electrons in each slice was

summed and averaged over the trajectory to obtain the electron density profile of the membranes as a function of *z*.

The center of the membrane is located at *z* = 0, so that values around ±2 nm correspond to the water – membrane interface, and values beyond ±3 nm are within the bulk solvent region. The leaflet that contains the cations is found in the region *z* < 0. The two maxima in each profile correspond to the location of the electron-rich phosphate groups. Several cation induced changes in the electron density profile can be observed. Firstly, it is apparent that the membrane thickness has changed. Comparing the distance between the two maxima in both profiles, it can be seen that the cation-bearing membrane contracted by about 0.6 nm. Secondly, the electron density at the center of the bilayer at around *z* = 0 of the cation-bearing membrane is somewhat increased as compared to the native membrane. As mentioned in section 3.3.1, a reduced membrane thickness can be attributed to curling of the phospholipid tails into the voids generated in the hydrophobic membrane region because of the shorter cation tails. This reorientation of the lipid tails reduces the small gap between the two leaflets and increases the density in the membrane center. Thirdly, it can be seen that around *z* = -2 nm, where the cations are located, these cations caused a substantial reduction of the electron density, in addition to the overall thinning effect. This reduction is not observed in the other leaflet at *z* = +2 nm and can be explained by the lack of expansion of the cations much beyond the phosphate groups once inserted, whereas the phospholipid head groups extend into the solvent. Lastly, it can be seen that around *z* = -1 nm, there is a dip in electron density as compared to the pure membrane. This region corresponds to the hydrophobic region of the membrane. The voids that are generated by the difference in alkyl chain lengths, as mentioned earlier, are located in this region, thereby reducing the electron density.

3.3.3 Lipid Order Parameters

The average orientation of the fatty acids of the phospholipids was studied by deriving their order parameters. Order parameters can be obtained from NMR experiments and also through MD simulations.[53] The order parameter S_{CD} is defined as follows:

$$S_{CD} = \frac{3}{2}\langle cos^2\theta \rangle - \frac{1}{2} \quad (7)$$

For a saturated carbon chain, the three atoms of each CH_2 group define a plane. The vectors perpendicular to the planes of two consecutive CH_2 groups in the carbon chain enclose the angle θ. By averaging over all occurring orientations θ, the parameter S_{CD} is obtained. Low values of S_{CD} indicate disorder, where all possible values of θ are realized with similar probabilities. A value of 1, on the other hand, represents the highest order, where all CH_2 planes are aligned in parallel. S_{CD} was determined for the oleoyl and palmitoyl chains in the POPE phospholipids, of the native and cation-bearing membrane, respectively. The results are shown in Figure 9. Qualitatively similar trends were observed for the POPG phospholipid (not shown).

A comparison of the order parameters shows that the overall orientation of both tail types was not greatly affected, as can be seen from the overall similarity of the curves. For instance, in the oleoyl tail, the sharp order increase at C10 compared to C9, which corresponds to the region of the cis double bond, remained the same. However, it is clear that insertion of the cations induced a significant decrease of the order parameters, especially farther away from the phosphate groups. In other words, cations caused disorder among the fatty acids in the bilayer. This finding is consistent with the previous observations of membrane thinning and increased density in the membrane center caused by $OMIM^+$. The voids generated by the short $OMIM^+$ alkyl chains allow fatty acid chains more flexibility and thus decrease their order.

3.4. Membrane Permeability of Small Polar Solutes

Changes in permeability of the cation-bearing membrane were compared the pure membrane. Ammonia was used as a probe that represents small polar solutes. The permeability was derived from two contributions: (1) The free energy changes that occurred during the movement of the probe along the reaction coordinate, ζ, through the membrane layers, which in turn are related to the local partition coefficients of the solute at particular values of ζ and (2)

the diffusivity of the solute at different membrane penetration depths ζ. The local partition coefficients and diffusion coefficients were combined to yield the permeability coefficient according to eqs. 2-5.

The free energy profile along ζ, which is the distance between the COMs of ammonia and the membrane bilayer projected onto the direction perpendicular to the membrane surface, where ζ = 0 corresponds to the membrane center, is shown in Figure 10. The free energy barrier is largest in the area |ζ| < 0.8 nm, i.e. in the hydrophobic core of the membrane, as expected for a polar solute. At the membrane center (ζ = 0), where the density of the membrane is lower, a dip in the free energy barrier is observed. The free energy barrier in the cation-bearing membrane is significantly lowered by about 5 kJ/mol over a wide range of ζ - values and also narrower than in the case of the pure membrane. The two free energy curves diverge from each other in the interval of -1.5 nm < ζ < -1 nm. This interval corresponds exactly to the area in which the cations are located. This finding indicates that the positive charge of $OMIM^+$, which is delocalized over large parts of the cation and reached somewhat into the membrane, provided favorable interactions with ammonia, thereby lowering the energy barrier. The reduced membrane thickness also leads to an overall smaller average distance of the ammonia molecule from the polar and charged components of the membrane during its passage, which is energetically favorable. For values ζ > -1 nm the two curves remain basically parallel to each other. This is a result of the similarity of the cation-bearing and the pure membrane in these membrane regions, where cations were not present.

In Figure 11, the diffusion coefficients of ammonia along the reactions coordinate ζ are shown. As expected, the diffusion coefficient of ammonia was greatly reduced in the polar region of the membrane and in the membrane – solvent interface area, compared to diffusion in the solvent. This can be explained by the tight packing of the polar parts of the phosphate lipids and stronger interactions between ammonia and lipids in this region. In the hydrophobic core region of the membrane, the diffusivity of ammonia increases and reaches a maximum at the center of the membrane at ζ = 0. This can be readily explained by the weak ammonia – lipid interactions, as well as a low lipid density that allows longer average mean paths between two scattering events of the small solute. Overall, the diffusivity profile closely corresponds to the electron density profile in Figure 8, so that high electron densities can be correlated with low solute diffusivities. It seems that the presence of the cations in the membrane did not influence the diffusivity of ammonia substantially. However, because of the cation induced membrane thinning, low diffusivities are limited to a smaller range of ζ–values as compared to the pure membrane. Also, the diffusivity maximum in the membrane center at ζ = 0 is less emphasized in the cation – bearing membrane because in this region, the density for cation-bearing membranes is somewhat higher as shown in Figure 8.

The results from Figures 10 and 11 were combined to derive the local membrane resistance along the reaction coordinate ζ, which is shown in Figure 12. The local resistance, $R(\zeta)$, has two distinct peaks around $|\zeta| = 0.9$ nm. The membrane area in which these peaks are located marks the transition from the polar part of the membrane to the hydrophobic core, where the passage of polar ammonia is energetically most unfavorable. A substantial reduction of the resistance in the cation-bearing membrane is observed.

The permeability coefficients with respect to ammonia were derived from eq 5 and are listed in Table 3. The permeability coefficient of the pure membrane has a value of $1.46 \pm 0.08 \cdot 10^{-5}$ cm/s, but is substantially increased by the inserted cations and yielded $10.1 \pm 0.8 \cdot 10^{-5}$ cm/s, which is a seven fold increase. According to the results discussed above, the cations facilitated permeation through the membrane because the delocalized positive charge of the inserted cations provided favorable interactions with ammonia and the short $OMIM^+$ alkyl chain led to a thinning of the membrane, thereby reducing the average distance of polar ammonia to the polar parts of the membrane during its passage through the hydrophobic membrane part. Additional changes in ammonia diffusivity induced by the inserted cations did not change permeation considerably. The substantial increase in permeation of the polar ammonia molecule suggests that cation insertion reduces the capability of the membrane to act as a permeability barrier, therefore suggesting an antimicrobial effect.

4. Conclusion

The effect of $OMIM^+$ insertions into a solvated membrane model was investigated with MD simulations using an empirical force field, where the phospholipid composition of the membrane was chosen so as to model the plasma membrane of *E. coli*.

A strong affinity of $OMIM^+$ for the lipid phase was observed. A favorable reduction in free energy of 9.6 kJ/mol was found, which translates to a 47 times larger concentration of cations inside the membrane than in the solvent at equilibrium. The $OMIM^+$ cations were oriented parallel to the phospholipid tails in the membrane, whereas the charge-carrying imidazolium ring remains partially solvated. Cation insertions were facilitated by ionic interactions between the positively charged imidazolium ring and the negatively charged phosphates of the lipids as well as hydrophobic effects that favors a transfer of the non-polar cation alkyl chain from water to the non-polar membrane core.

The free energy potential of two $OMIM^+$ inside the membrane was derived as a function of their COM distance. Two cations that diffuse laterally towards each other will encounter a slight barrier of 4.2 kJ/mol caused by cation - cation repulsion, after which a free energy minimum at

a distance of 1.3 nm is reached. In this free energy minimum, the two cation imidazolium rings are separated from each other by negatively charged lipid phosphates, so that $OMIM^+$ – phosphate – $OMIM^+$ coordination patterns emerges. This coordination is favored by 5.9 kJ/mol compared to two separated cations inside the membrane. Dissociation of this coordination requires 10.1 kJ/mol. This significant effective cation attraction suggests a certain tendency of cations to aggregate in the membrane, which could potentially aggravate the disruptive effect of cations on the membrane.

Cations were inserted into one leaflet of the membrane bilayer at mutual distances that corresponded to the energetically most favorable cation – cation distance that was found in the preceding free energy analysis. The roughness of the membrane surface was not much affected by the cations but appears to increase slightly. However, it was found that the cation insertions caused a membrane thinning of 0.6 nm according to calculated electron density profiles (0.2 nm according to the average positions of phosphorous atoms in the two leaflets). The membrane thinning was caused by the shorter length of the cation alkyl chains compared to the fatty acids of the lipids, which generated voids in the membrane that in turn enabled a mutual approach of the two leaflets. These generated voids were also confirmed by a reduction of the electron density profiles in the membrane region where the cation alkyl chains terminated. Due to the cation induced membrane thinning, the membrane density was somewhat increased in the region of the membrane center (around z = 0). Additionally, the density of the modified membrane also decreased in the region of the membrane – solvent interface, because of the small size of the cation ring compared to the phospholipid head groups that extend into the solvent. A comparison of the lipid order parameters showed that the insertion of cations into the membrane induced additional disordering of the fatty acids because the generated voids allowed neighboring fatty acids to flex into these voids, hence reducing their tendency to be oriented straight and perpendicularly to the membrane surface.

An analysis of the effect of cations inside the membrane on the permeation of ammonia revealed a substantial increase of the permeability coefficient by a factor of seven. This increase in permeability was caused by a reduction of membrane resistance in the transition zone from the polar membrane region to the hydrophobic core. The permeation was facilitated by the delocalized positive charge on $OMIM^+$ that partially extended into the hydrophobic part of the membrane, thereby providing favorable interactions with polar ammonia. Moreover, the thinning of the membrane layer caused by the cations reduced the average distance between the ammonia solute and the polar membrane regions during the passage through the membrane, thereby reducing the associated overall free energy barrier. It appears to be likely that a qualitatively similar behavior could be obtained for other small polar solutes.

Overall, the observed propensity of $OMIM^+$ for membrane insertion, the indicated tendency of these amphiphilic cations to aggregate inside the membrane and the substantially facilitated permeation of ammonia suggest an antimicrobial effect that could disrupt the functioning of the bacterial membrane. A cation induced improved permeation of small polar solutes across the membrane suggests that vital compounds could leak out of the cell, whereas harmful compounds could enter, thereby affecting the homeostasis of the cell. Thus, the results reveal why certain ILs are found to be toxic at sufficiently large concentrations, especially those that carry longer lipophilic alkyl chains.

Acknowledgments

We gratefully acknowledge the provision of computational facilities by the A*STAR Computational Resource Centre of Singapore (ACRC) and the Institute of High Performance Computing (IHPC) as well as the financial support from the Joint Council Office (JCO) of the Agency for Science, Technology and Research (A*STAR) of Singapore**.**

References

1 R. D. Rogers, K. R. Seddon, *Science*, 2003, **302**, 792-793.
2 R. A. Sheldon, R. M. Lau, M. J. Sorgedrager, F. v. Rantwijk, K. R. Seddon, *Green Chem.*, 2002, **4**, 147–151.
3 M. Petkovic, K. R. Seddon, L. P. N. Rebelo, C. S. Pereira, *Chem. Soc. Rev.*, 2011, **40**, 1383-1403.
4 H. Olivier-Bourbigou, L. Magna, D. Morvan, *Appl. Catal. A*, 2010, **373**, 1-56.
5 N. V. Plechkova, K. R. Seddon, *Chem. Soc. Rev.*, 2008, **37**, 123-150.
6 D. Coleman, M. Špulák, M. T. Garcia, N. Gathergood, *Green Chem.*, 2012, **14**, 1350-1356.
7 K. M. Docherty, J. Charles F. Kulpa, *Green Chem.*, 2005, **7**, 185–189.
8 B. F. Gilmore, *Antimicrobial Ionic Liquids*, in: P.A. Kokorin (Ed.) Ionic Liquids: Applications and Perspectives, InTech, Rijeka, Croatia, 2011, 587-604.
9 J. Łuczak, C. Jungnickel, I. Łacka, S. Stolte, J. Hupka, *Green Chem.*, 2010, **12**, 593–601.
10 Y. V. Nancharaiah, G. K. K. Reddy, P. Lalithamanasa, V. P. Venugopalan, *Biofouling*, 2012, **28**, 1141–1149.
11 J. Pernak, K. Sobaszkiewicz, I. Mirska, *Green Chem.*, 2003, **5**, 52–56.

12 A. Cornellas, L. Perez, F. Comelles, I. Ribosa, A. Manresa, M. T. Garcia, *J. Colloid Interface Sci.*, 2011, **355** 164–171.
13 B. J. Denny, L. Novotny, P. W. J. West, M. Blesova, J. Zamocka, *Med. Princ. Pract.*, 2005, **14**, 377–381.
14 V. Kumar, S. V. Malhotra, *Bioorg. Med. Chem. Lett.*, 2009, **19**, 4643–4646.
15 S. P. M. Ventura, C. S. Marques, A. A. Rosatella, C. A. M. Afonso, F. Goncalves, J. A. P. Coutinho, *Ecotox. Environ. Safe.*, 2012, **76**, 162-168.
16 L. Carson, P. K. W. Chau, M. J. Earle, M. A. Gilea, B. F. Gilmore, S. P. Gorman, M. T. McCann, K. R. Seddon, *Green Chem.*, 2009, **11**, 492–497.
17 S. Stolte, M. Matzke, J. Arning, A. Böschen, W.-R. Pitner, U. Welz-Biermann, B. Jastorff, J. Ranke, *Green Chem.*, 2007, **9**, 1170–1179.
18 S. Morrissey, B. Pegot, D. Coleman, M. T. Garcia, D. Ferguson, B. Quilty, N. Gathergood, *Green Chem.*, 2009, **11**, 475–483.
19 E. Egberts, S. J. Marrink, H. J. C. Berendsen, *Eur. Biophys. J. Biophy.*, 1994, **22**, 423-436.
20 S. J. Marrink, H. J. C. Berendsen, *J. Phys. Chem.*, 1996, **100**, 16729-16738.
21 D. P. Tieleman, S. J. Marrink, H. J. C. Berendsen, *Biochim. Biophys. Acta*, 1997, **1331**, 235-270.
22 D. J. Tobias, K. C. Tu, M. L. Klein, *Curr. Opin. Colloid Interface Sci.*, 1997, **2**, 15-26.
23 R. J. Bingham, P. Ballone, *J. Phys. Chem. B*, 2012, **116**, 11205–11216.
24 M. Klähn, M. Zacharias, *Phys. Chem. Chem. Phys.*, 2013, **15**, 14427-14441.
25 B. Yoo, J. K. Shah, Y. Zhu, E. J. Maginn, *Soft Matter*, 2014, **10**, 8641–8651.
26 G. S. Lim, J. Zidar, D. W. Cheong, S. Jaenicke, M. Klähn, *J. Phys. Chem. B*, 2014, **118**, 10444−10459.
27 R. F. Epand, M. A. Schmitt, S. H. Gellman, R. M. Epand, *Biochim. Biophys. Acta*, 2006, **1758**, 1343–1350.
28 P. L. Yeagle, *The Membranes of Cells*, 2nd ed., Academic Press, San Diego, 1993.
29 S. Jo, T. Kim, W. Im, *Plos One*, 2007, **2**, e880
30 S. Jo, T. Kim, V. G. Iyer, W. Im, *J. Comput. Chem.*, 2008, **29**, 1859-1865.
31 S. Jo, J. B. Lim, J. B. Klauda, W. Im, *Biophys. J.*, 2009, **97**, 50-58.
32 E. L. Wu, X. Cheng, S. Jo, H. Rui, K. C. Song, E. M. Dávila-Contreras, Y. Qi, J. Lee, V. Monje-Galvan, R. M. Venable, J. B. Klauda, W. Im, *J. Comput. Chem.*, 2014, **35**, 1997-2004
33 R. W. Pastor, A. D. MacKerell Jr., *J. Phys. Chem. Lett.*, 2011, **2**, 1526-1532.
34 M. T. Hyvonen, P. T. Kovanen, *Eur. Biophys. J. Biophy.*, 2005, **34**, 294-305.
35 L. Janosi, A. A. Gorfe, *J. Chem. Theory Comput.*, **6**, 3267-3273.
36 J. B. Klauda, R. M. Venable, J. A. Freites, J. W. O'Connor, D. J. Tobias, C. Mondragon-Ramirez, I. Vorobyov, A. D. MacKerell Jr., R. W. Pastor, *J. Phys. Chem. B*, 2010, **114**, 7830-7843.
37 T. J. Piggot, Á. Piñeiro, S. Khalid, *J. Chem. Theory Comput.*, 2012, **8**, 4593–4609.
38 K. Vanommeslaeghe, E. Hatcher, C. Acharya, S. Kundu, S. Zhong, J. Shim, E. Darian, O. Guvench, P. Lopes, I. Vorobyov, A. D. MacKerell Jr., *J. Comput. Chem.*, 2010, **31**, 671-690.
39 W. L. Jorgensen, J. Chandrasekhar, J. D. Madura, R. W. Impey, M. L. Klein, *J. Chem. Phys.*, 1983, **79**, 926-935.
40 B. Hess, C. Kutzner, D. van der Spoel, E. Lindahl, *J. Chem. Theory Comput.*, 2008, **4**, 435-447.
41 D. van der Spoel, E. Lindahl, B. Hess, G. Groenhof, A. E. Mark, H. J. C. Berendsen, *J. Comput. Chem.*, 2005, **26**, 1701-1718.

42 B. Hess, H. Bekker, H. J. C. Berendsen, J. Fraaije, *J. Comput. Chem.*, 1997, **18**, 1463-1472.
43 W. G. Hoover, *Phys. Rev. A*, 1985, **31**, 1695-1697.
44 S. Nose, *J. Chem. Phys.*, 1984, **81**, 511-519.
45 M. Parrinello, A. Rahman, *J. Appl. Phys.*, 1981, **52**, 7182-7190.
46 M. P. Allen, D. J. Tildesley, *Computer simulations of liquids*, Oxford Science Publications, Oxford, 1987.
47 T. Darden, D. York, L. Pedersen, *J. Chem. Phys.*, 1993, **98**, 10089-10092.
48 U. Essmann, L. Perera, M. L. Berkowitz, T. Darden, H. Lee, L. G. Pedersen, *J. Chem. Phys.*, 1995, **103**, 8577-8593.
49 S. Kumar, J. M. Rosenberg, D. Bouzida, R. H. Swendsen, P. A. Kollman, *J. Comput. Chem.*, 1992, **13**, 1011–1021.
50 J. S. Hub, B. L. de Groot, D. van der Spoel, *J. Chem. Theory Comput.*, 2010, **6**, 3713-3720.
51 S. J. Marrink, H. J. C. Berendsen, *J. Phys. Chem.*, 1994, **98**, 4155-4168.
52 D. Bemporad, J. W. Essex, C. Luttmann, *J. Phys. Chem. B*, 2004, **108**, 4875-4884.
53 L. S. Vermeer, B. L. d. Groot, V. Réat, A. Milon, J. Czaplicki, *Eur. Biophys. J.*, 2007, **36**, 919–931.

Table 1: Free Energy Change of $OMIM^+$ Extraction from Membrane at Different Distances to a Neighboring Second Cation[a]

$r_{cat\text{-}cat}$ [nm]	ΔG_{ins}[b] [kJ/mol]
0.94	13.5 (1.2)
1.25[c]	15.5 (0.7)
1.50	6.5 (1.2)

[a] The negative values of these free energy changes are cation insertion free energies as encountered in section 3.1.

[b] The standard errors were calculated with the Bootstrap method and are given in parenthesis.

[c] Optimal distance between cations in membrane. The resulting free energy change of 15.5 kJ/mol corresponds to ΔG_1 in the TDC shown in Figure 5.

Table 2: Thickness, Roughness, Surface Area per Molecule, and Total Surface Area of the Cation-Bearing and Pure Membrane[a]

	d[b] [nm]	r_m[c] [nm]	$A_{mol\text{-}surf}$ [nm^2]	$A_{tot\text{-}surf}$ [nm^2]
Membrane + IL	4.1_1	0.206_5	0.530_3	24.0_1
Pure membrane	4.31_9	0.192_7	0.560_8	22.0_1

[a] Statistical errors are given as subscripts.

[b] Membrane thickness was obtained from the difference between the average z-coordinate of phosphorus atoms in the two leaflets.

[c] Membrane surface roughness was determined using eq 6 for the leaflet that contained the cations.

Table 3: Permeability Coefficients of Membranes with Respect to Ammonia[a]

	P [10^{-5} cm/s]
Membrane + IL	10.1_8
Pure membrane	1.46_8

[a] Statistical errors were derived with the Bootstrap method and error propagation and are given as subscripts.

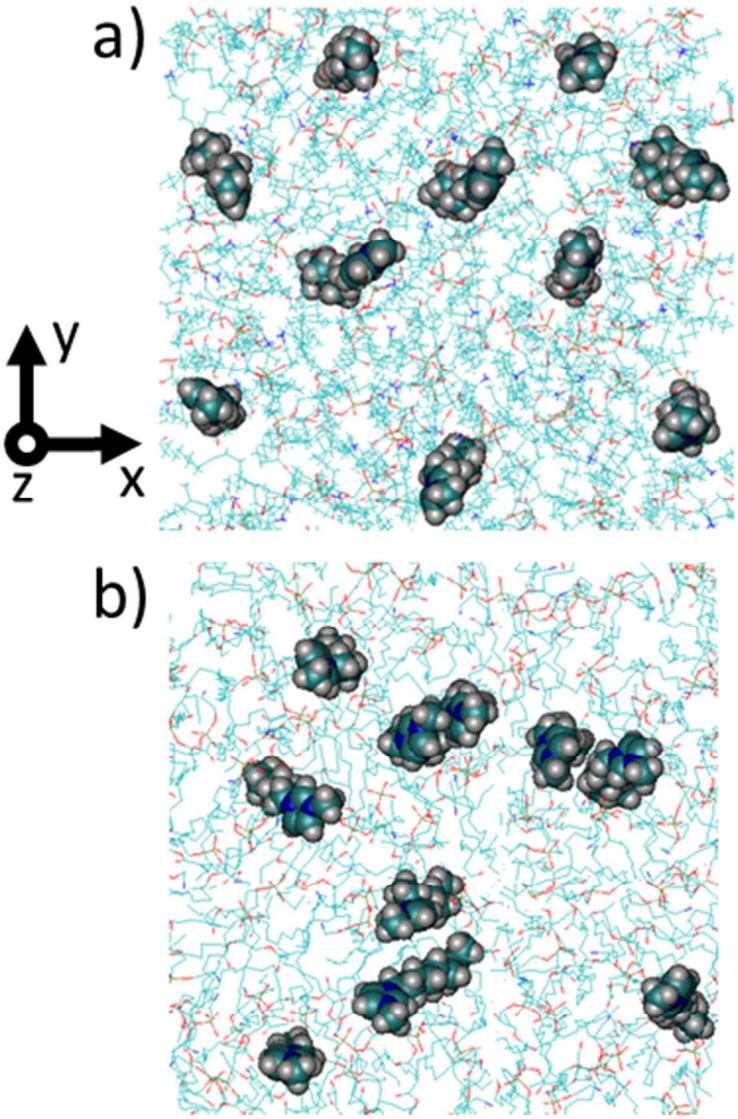

Figure 1: (a) Initial distribution of $OMIM^+$ in the membrane layer and (b) a representative cation distribution at the equilibrium (seen from top). The IL cations are highlighted with a van der Waals representation, whereas the phospholipids are shown in a stick representation. The display of solvent was omitted for clarity. Color code: H = white, C = turquoise, N = blue and O = red.

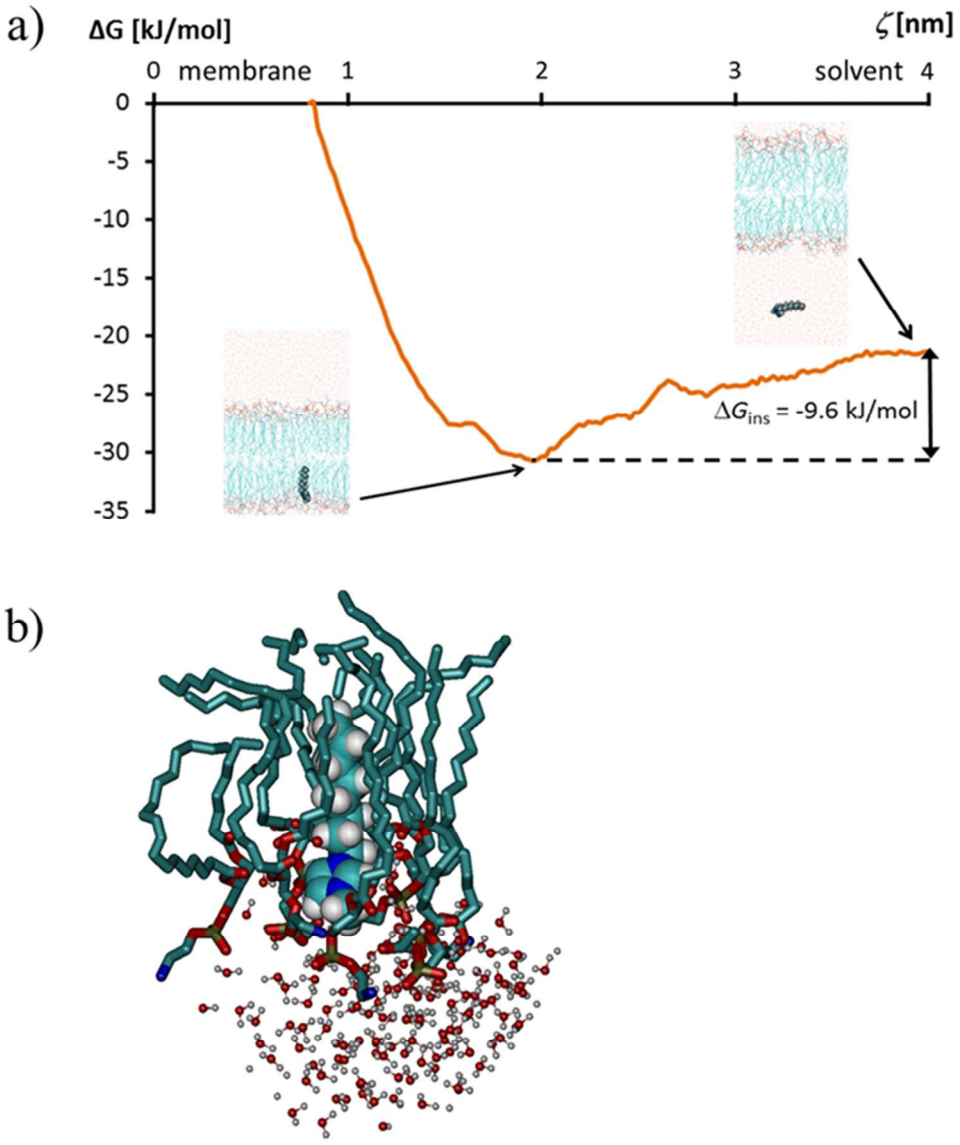

Figure 2: (a) Free energy profile, $\Delta G(\zeta)$, for transfer of $OMIM^+$ from solvent into the membrane. The reaction coordinate ζ is defined as the distance between the centers-of-masses of cation and membrane, projected onto z-direction. The $OMIM^+$ position in the solvent and in the membrane at the minimum of free energy are shown in the insets, respectively. (b) A representative equilibrated structure that shows the coordination of inserted $OMIM^+$ with neighboring phospholipids at the free energy minimum. The phospholipids are shown in licorice representation, whereas inserted $OMIM^+$ is highlighted with van der Waals spheres. Water in the vicinity of $OMIM^+$ is also displayed. Hydrogens on the phospholipids were omitted for clarity. Color code: H = white, C = turquoise, N = blue, O = red and P = brown.

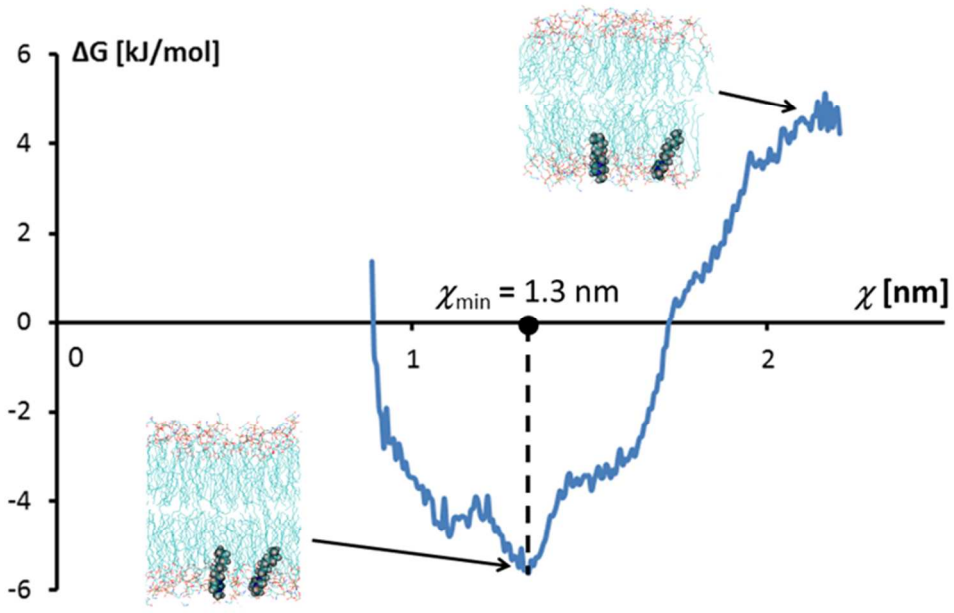

Figure 3: Free energy profile, $\Delta G(\chi)$, for moving $OMIM^+$ within the membrane relative to a second inserted $OMIM^+$. The reaction coordinate χ is defined as the cation – cation center-of-mass distance projected onto the xy - membrane plane. A clear minimum at χ = 1.3 nm was obtained. The $OMIM^+$ positions in the membrane at the minimum of free energy and when separated are shown in the insets, respectively.

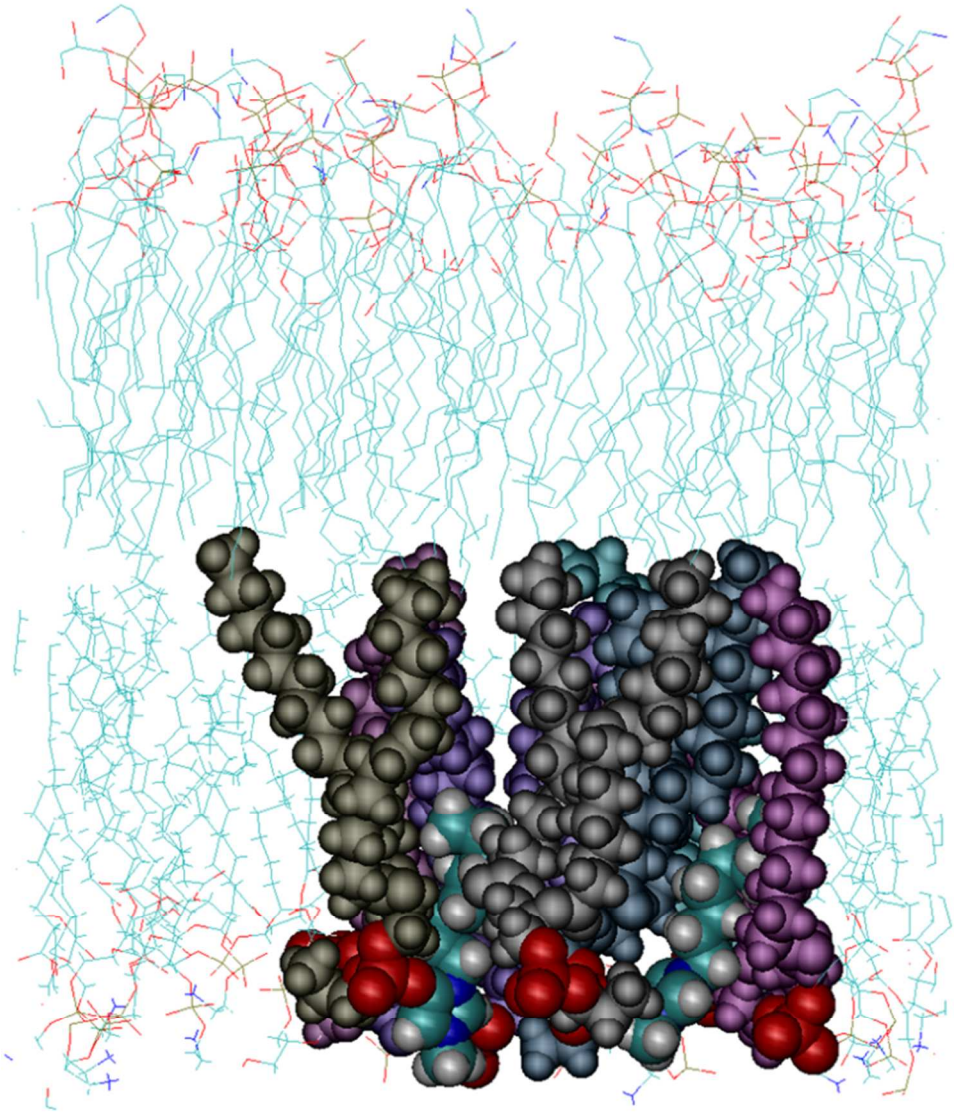

Figure 4: A representative equilibrated structure of two inserted $OMIM^+$ with neighboring phospholipids at the free energy minimum. A close proximity of $OMIM^+$ rings and lipid phosphates to form an $OMIM^+$ – phosphate – $OMIM^+$ coordination pattern can be observed. The phospholipids are coloured in different shades of purple and grey with their phosphate groups highlighted in red. For cations and the rest of the system the standard colour code was used (H = white, C = turquoise, N = blue and O = red). The display of obstructing phospholipids was omitted for clarity.

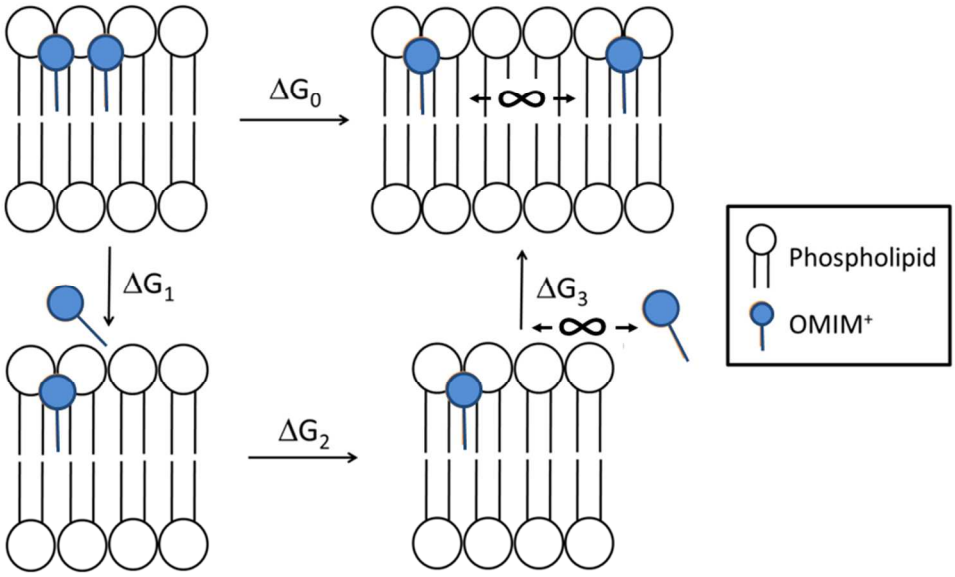

Figure 5: Scheme of thermodynamic cycle used to derive free energy changes for separating two neighboring inserted cations from each other, $\Delta G_0 = \Delta G_{assoc}$.

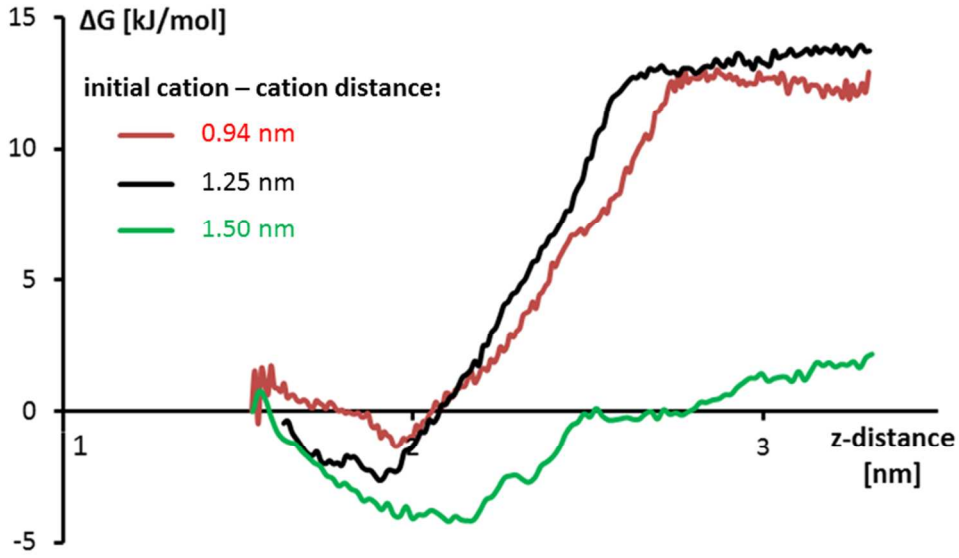

Figure 6: Free energy profile, $\Delta G(\zeta)$, for extracting $OMIM^+$ from the membrane to the solvent, while a second $OMIM^+$ remained in the membrane. The reaction coordinate ζ is defined as the COM distance between the cation and the membrane projected onto the direction perpendicular to the membrane surface. The initial distance between the two cation COMs in the membrane was 0.94 nm (red), 1.25 nm, which is the optimal distance (black), and 1.50 nm (green).

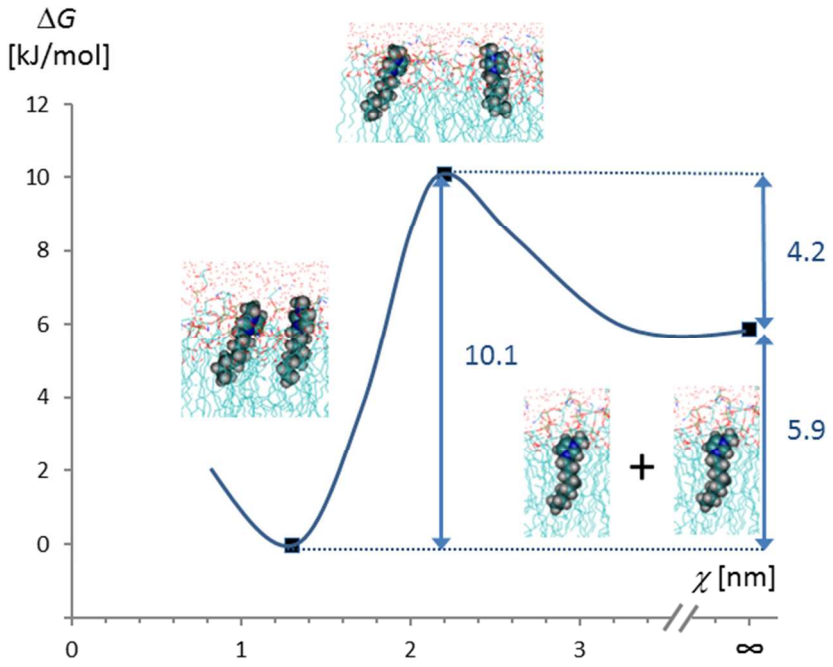

Figure 7: Free energy barrier for formation (4.2 kJ/mol) and dissociation (10.1 kJ/mol) of a $OMIM^+$ – phosphate – $OMIM^+$ coordination in the membrane. The association free energy of the two cations is ΔG_{assoc} = 5.9 kJ/mol.

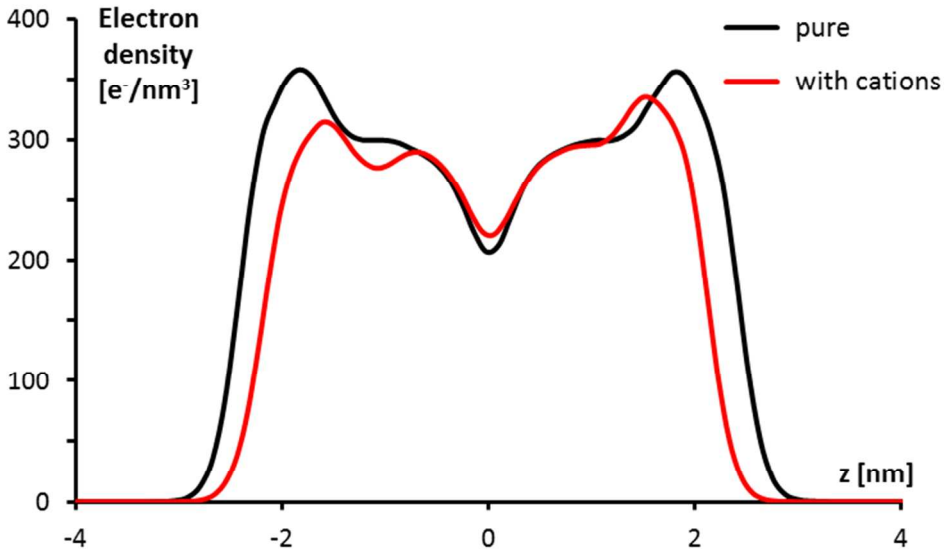

Figure 8: Membrane electron density profiles in the direction perpendicular to the membrane surface, *z*, of the cation-bearing system (red) compared to the electron profile of the pure membrane (black). The center of the membrane is located at $z = 0$. Cations were inserted into the layer that corresponds to negative values of ζ.

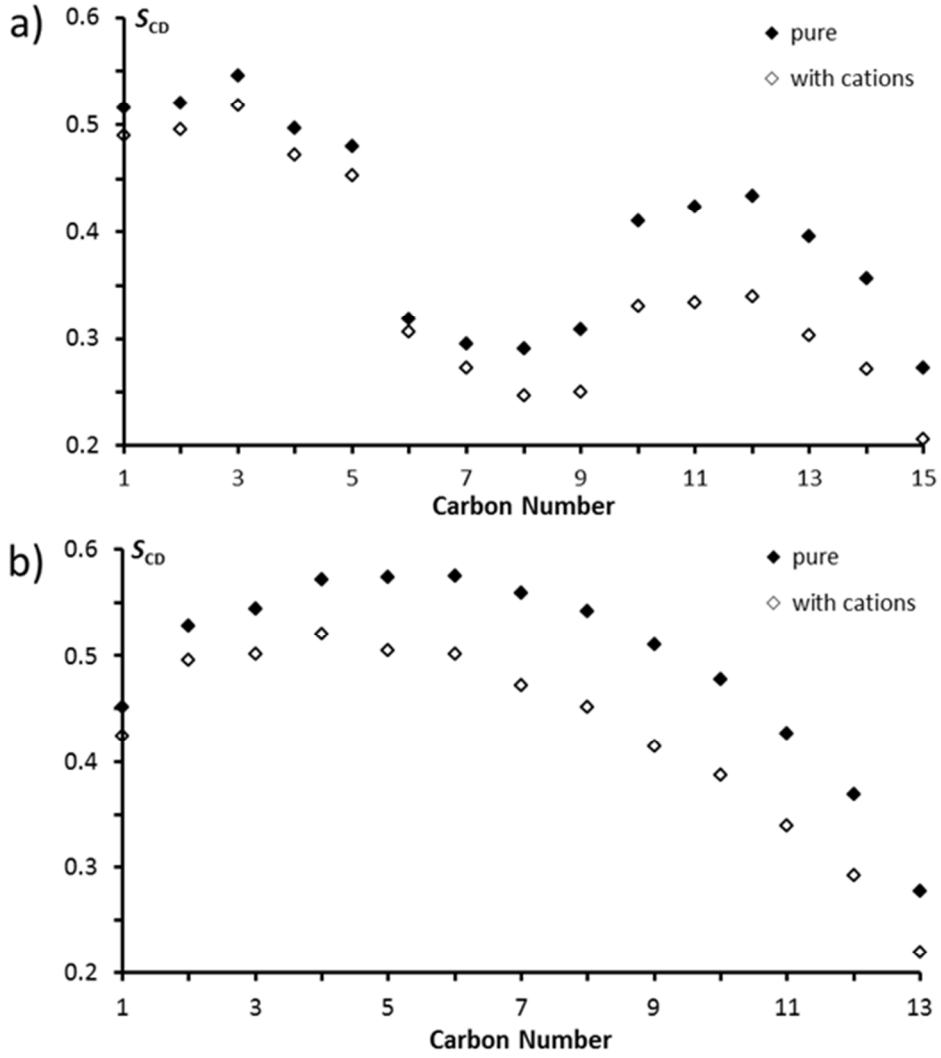

Figure 9: Deuterium order parameters, S_{CD}, of oleoyl (a) and palmitoyl (b) fatty acids in the lipid POPE for the pure (filled diamonds) and cation-bearing (empty diamonds) membrane. Carbon 1 represents the carbon closest to the polar head group and the last carbon refers to the carbon adjacent to the terminal methyl group.

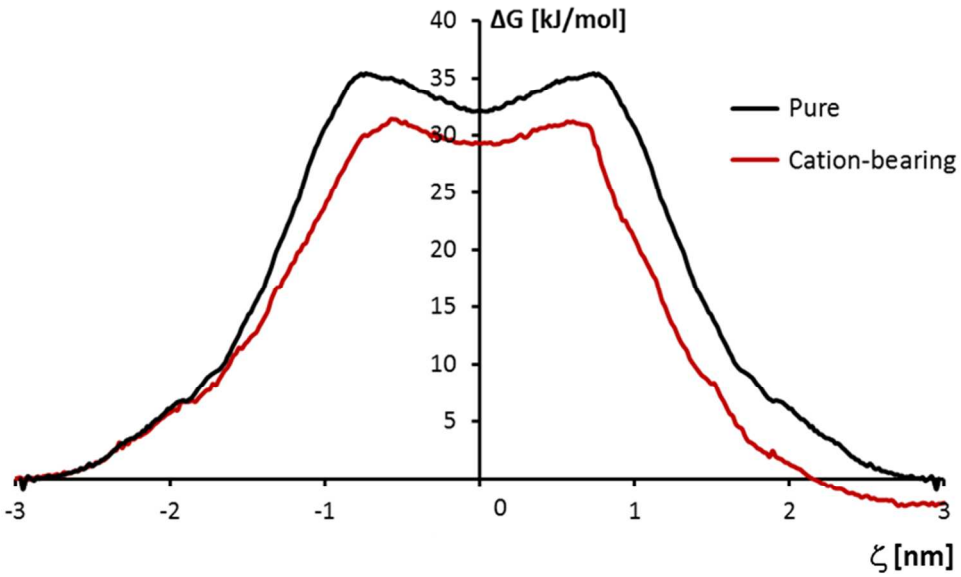

Figure 10: Free energy profile, $\Delta G(\zeta)$, for the permeation of ammonia through the pure membrane (black) and the cation-bearing membrane (red). The reaction coordinate ζ is defined as the COM distance between ammonia and the membrane, projected onto the direction perpendicular to the membrane surface. The center of the membrane is at $\zeta = 0$. Cations were inserted into the layer that corresponds to negative values of ζ.

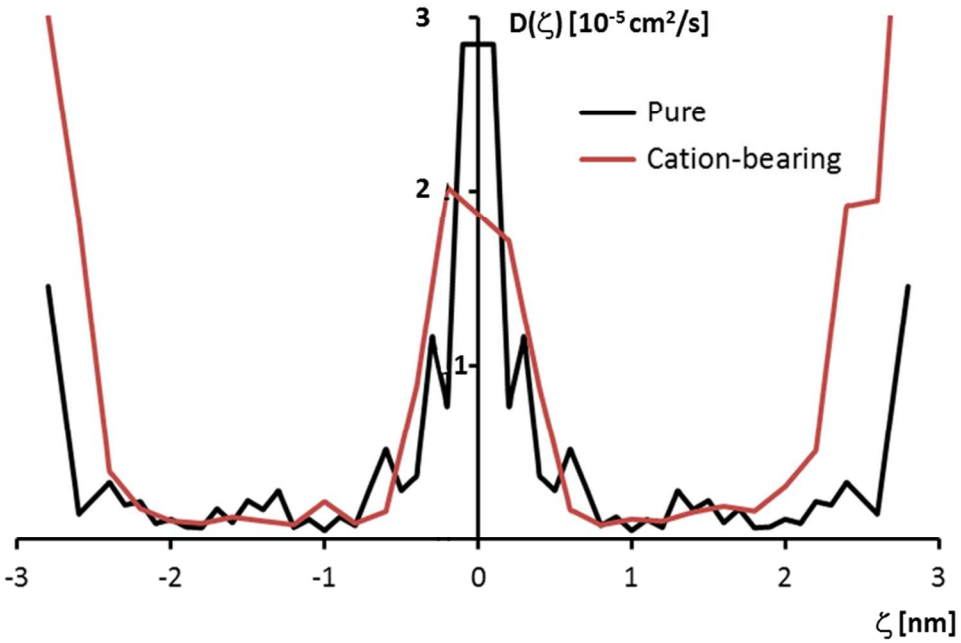

Figure 11: Diffusion coefficients, *D*(ζ), of ammonia at different penetration depths ζ in the pure membrane (black) and the cation-bearing membrane (red). The reaction coordinate ζ is defined as the COM distance between ammonia and the membrane, projected onto the direction perpendicular to the membrane surface. The center of the membrane is at ζ = 0. Cations were inserted into the layer that corresponds to negative values of ζ.

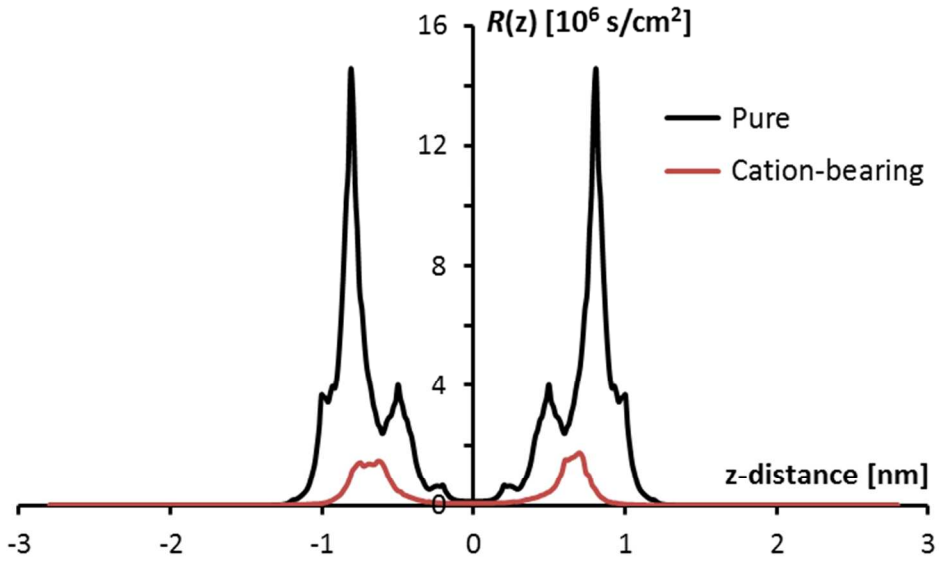

Figure 12: Local resistance, $R(\zeta)$, of the pure membrane (black) and cation-bearing membrane (red) with respect to the permeation of ammonia at different penetration depths ζ. The reaction coordinate ζ is defined as the COM distance between ammonia and the membrane, projected onto the direction perpendicular to the membrane surface. The center of the membrane is at $\zeta = 0$. Cations were inserted into the layer that corresponds to negative values of ζ.

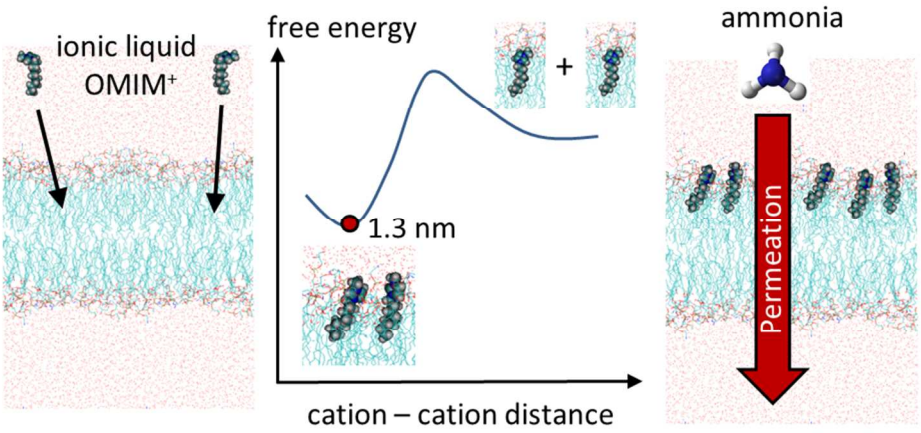

Table of contents graphics